Jestr

Journal of Engineering Science and Technology Review 17 (4) (2024) 164-170

Research Article

JOURNAL OF
Engineering Science and Technology Review

www.jestr.org

A Concrete-filled Steel Pipe Composite Segment for Shield Tunnel in Complex Geological Conditions

Baosheng Dong*

CCCC First Highway Engineering Xiamen Engineering Co. Ltd., Xiamen 361000, China

Received 12 May 2024; Accepted 26 August 2024

Abstract

The traditional segment always experiences gradual performance degradation during its service life in complex geological conditions, which results in numerous problems in the form of large deformations, seepage, and concrete cracking. Therefore, a new type of composite segment was proposed, in which an arc-shaped concrete-filled steel pipe component is embedded. A numerical model of the proposed segment under three-point bending conditions was developed and subsequently validated through laboratory tests. A parametric study was also conducted, encompassing the dimensions and locations of the arc-shaped concrete-filled steel pipe component. The results indicate that the new composite segment can effectively enhance the segment's load-bearing capacity, and both the yield and ultimate loads of the segment can be increased. Additionally, the parametric study revealed that the thickness and diameter of the pipe do not have a significant impact on the segment's load-bearing capacity, and the position of the pipe does not affect the mechanical performance of the segment. The proposed segment can potentially be used to replace traditional segments in complex geological conditions.

Keywords: Shield tunnel, Composite segment, Concrete-filled steel tubular structure, Ultimate load capacity

1. Introduction

With the continuous development of tunnel construction equipment, the number of tunnels constructed via the shield method has been increasing, and the shield method has become the prevalent technology for shield tunnel construction due to its convenience and speed [1-3]. However, as the number of tunnels grows, shallow underground space has gradually become overcrowded, and the utilization of underground space has shifted from shallow depths to deeper levels, with geological conditions becoming increasingly complex. Furthermore, rectangular and other non-circular cross-sectional shapes are currently being used instead of circular cross-sections to enlarge the tunnels' cross-sectional areas. In these complex geological conditions, the bolts connecting shield tunnel segments become more sensitive to surrounding conditions during the construction process. In special cases, hydraulic and earth pressures within the tunnels have increased, which necessitates improved performance from the shield tunnel segments [4, 5].

The traditional tunnel segments, particularly in shield tunnels, often face a gradual decline in their structural performance over their service life. This degradation can manifest in various forms, such as extensive concrete cracking, reinforcement bar corrosion, and a general weakening of the material properties. These issues not only compromise the integrity of the tunnel but also pose significant safety risks. In extreme cases, the accumulated damage can lead to catastrophic failures, including large transverse deformations that threaten the stability of the entire tunnel structure. Furthermore, shield tunnels are often subjected to dynamic and unpredictable external environmental factors, such as soil movements, groundwater fluctuations, and seismic activities. These factors can exacerbate the aging process in specific areas, causing localized weaknesses and further reducing the overall structural performance. The risk of large deformations increases exponentially under such conditions, making it imperative to address these issues proactively. Currently, when the deformation of tunnel segments exceeds acceptable standards, a popular method of reinforcement involves bonding external materials, such as steel or fiber reinforced polymers, to the existing segments [6, 7]. This technique offers the advantages of speed and simplicity, allowing for relatively quick and cost-effective repairs. However, the effectiveness of this reinforcement heavily relies on the quality of the bond between the external plates and the segment.

Unfortunately, the bond interface is often considered the Achilles' heel of these reinforced segments. Interfacial debonding, either due to improper installation, inadequate material compatibility, or environmental factors, can lead to sudden and catastrophic failures. Such failures not only undermine the purpose of the reinforcement but also introduce new safety hazards, as the detached plates can become projectiles within the confined space of the tunnel. It is also worth noting that external reinforcement is essentially a remedial measure, addressing the symptoms rather than the root causes of the problem. It often requires the tunnel to be closed for extended periods during the strengthening process, causing disruptions to traffic and potentially impacting the local economy [8, 9]. Additionally, the installation of external plates can reduce the available spacing within the tunnel, limiting its capacity to accommodate future infrastructure upgrades or emergency services.

*E-mail address: 19715005@qq.com
ISSN: 1791-2377
doi:10.25103/jestr.174.18

Given these limitations, there is a pressing need to develop innovative tunnel segments specifically designed for complex geological conditions. These new segments should be engineered to withstand the challenges posed by dynamic external environments while maintaining structural integrity and performance over their extended service lives. Advanced materials, such as high-performance concretes, corrosion-resistant reinforcements, and durable bonding agents, could be incorporated into the design to enhance durability and resilience.

2. State of the art

To achieve a high load capacity for shield tunnel lining segments subjected to high water pressure and earth pressure deep underground, various composite segments have been developed. For example, Nishikawa proposed a prestressed lining segment structure that utilizes fewer steel bars and conserves bolts, thereby reducing production costs and construction labor for the segment. However, this type of segment is more suitable for the construction of medium- to large-span tunnels rather than small-span tunnels [10]. Vion and Joing discussed the development of construction equipment for single-track decks and the interaction between U-shaped structural design and construction equipment [11, 12]. Zhao et al. simulated the behavior of an steel fiber reinforced concrete (SFRC) segment under thrust loads and found that SFRC materials can enhance tensile strength to prevent concrete cracking [13].

Other researchers, such as Yang and their team, delved deeper into the mechanical prowess of carbon fiber reinforced concrete (CFRC) segments through the utilization of an innovative 3D mesoscale numerical model. This sophisticated model incorporated the randomness of steel fiber distribution, a crucial aspect that significantly impacts the material's overall performance [14]. By simulating the intricate interactions between the carbon fibers, cement matrix, and randomly interspersed steel fibers, the study provided a nuanced understanding of CFRC's mechanical behavior under various loading conditions

Incorporating steel fibers into ultra-high-performance concrete (UHPC) not only enhances its hardening characteristics but also acts as a formidable barrier against crack propagation. This phenomenon is attributed to the fibers' ability to bridge across cracks, effectively dissipating energy and delaying the onset of failure [15-17]. Consequently, UHPC exhibits remarkable improvements in its mechanical attributes, foremost among them being its heightened cracking resistance, superior deformation capacity, and exceptional damage tolerance [18-20]. These traits make UHPC an ideal candidate for structures requiring unparalleled strength and durability. Given these advantages, UHPC has garnered significant attention as a potential replacement for traditional lining segments in infrastructure projects, including tunnels, bridges, and building facades [21-23]. The adoption of UHPC has been driven by its ability to significantly reduce maintenance costs, enhance structural safety, and extend service life. However, while existing methods aimed at reinforcing traditional segments have made strides in mitigating construction-induced cracking, they have yet to achieve a substantial elevation in the ultimate load-bearing capacity of these structures.

The synergistic effects of combining UHPC with advanced reinforcement techniques could be explored, such as the use of hybrid fiber reinforcement or innovative reinforcement geometries. Additionally, investigating the long-term performance of UHPC-based structures under extreme environmental conditions and dynamic loading scenarios would provide invaluable insights into their durability and reliability. Ultimately, such endeavors could pave the way for the widespread adoption of UHPC as the material of choice for constructing resilient and sustainable infrastructure [24-26].

It is widely recognized that concrete-filled steel tube (or pipe) structures optimally combine the strengths of both steel and concrete, such as high ductility, strength, and stiffness [27-30]. In this study, an arc-shaped concrete-filled steel pipe (ASCFSP) component was combined with an ordinary segment to design a novel composite segment for shield tunnel construction under complex geological conditions. This study modeled the proposed segment using the ABAQUS program. The numerical method was subsequently validated, and a parametric study was also undertaken.

The structure of this study is organized as follows. In Section 3, the material model for the segment is introduced. In Section 4, the numerical model for the proposed segment is developed and verified by tests. And then conclusions are listed in Section 5.

3. Methodology

3.1 Material model

3.1.1 Steel

In this work, a double-broken line elastoplastic model was adopted for the steel bar, steel pipe and bolt. The elastoplastic constitutive relationship of this model consisted of two straight lines, and the stress-strain curve of the steel was simplified, which was different from the actual stress-strain situation of the steel. However, the simplified model could provide a quick calculation speed and overcome the difficulty of convergence. The steel's stress-strain response is shown in Fig. 1, where f_y is the steel's yield strength, f_y and ε_y are the strength and strain at yielding point for the steel material, respectively. The modulus of the steel after yielding is replaced by $0.01E_s$.

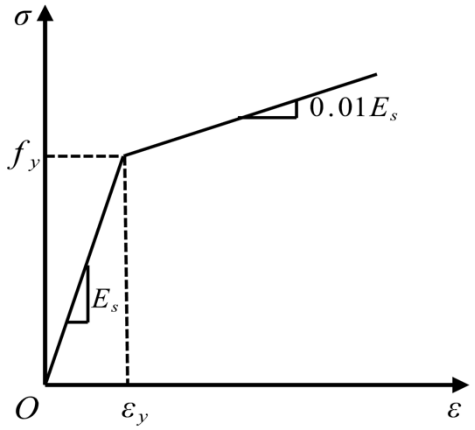

Fig. 1. Stress-strain curve of the steel

3.1.2 Concrete

According to the China Design Code of the Concrete Structure, the stress-strain response of the concrete material subjected to tension can be described by:

$$\sigma = (1-d_t)E_c\varepsilon \tag{1}$$

$$d_t = \begin{cases} 1-\rho_t\left[1.2-0.2x^5\right], x\tilde{N}1 \\ 1-\dfrac{\rho_t}{\alpha_t(x-1)^{1.7}+x}, x>1 \end{cases} \tag{2}$$

$$x = \frac{\varepsilon}{\varepsilon_{t,r}} \tag{3}$$

$$\rho_t = \frac{f_{t,r}}{E_c\varepsilon_{t,r}} \tag{4}$$

where α_t represents the value that determines the descent stage of the curve of the concrete. $f_{t,r}$ is the tensile strength, which can be adjusted as f_t, $f_{t,k}$ or $f_{t,m}$ according to needs. $\varepsilon_{t,r}$ is the strain at the tensile strength $f_{t,r}$. d_t is the damage parameter for the concrete subjected to tension.

The strength grade of the concrete used in this study is C50, and the parameters for α_t, $f_{t,r}$, $\varepsilon_{t,r}$ and E_c are 2.12, 2.64 MPa, 0.00109 and 34.5 GPa.

The stress-strain response for the concrete subjexted to uniaxial compression can be described by Eq. (5):

$$\sigma = (1-d_c)E_c\varepsilon \tag{5}$$

$$d_t = \begin{cases} 1-\dfrac{\rho_c n}{n-1+x^n}, x \le 1 \\ 1-\dfrac{\rho_c}{\alpha_c(x-1)^2+x}, x>1 \end{cases} \tag{6}$$

$$\rho_c = \frac{f_{c,r}}{E_c\varepsilon_{c,r}} \tag{7}$$

$$n = \frac{E_c\varepsilon_{c,r}}{E_c\varepsilon_{c,r}-f_{c,r}} \tag{8}$$

$$x = \frac{\varepsilon}{\varepsilon_{c,r}} \tag{9}$$

where α_c is the parameter controlling the descending stage of compressive responses of the concrete. $f_{c,r}$ is the strength of the concrete subjected to compression, which can be also adjusted as f_c, $f_{c,k}$ or $f_{c,m}$ according to needs. $\varepsilon_{c,r}$ is the compressive strain at the compressive strength $f_{c,r}$. d_c is the damage parameter for the concrete under compression.

The stress-strain response of the concrete subjected to the uniaxial tension and compression is presented in Fig. 2.

3.2 New composite segment

3.2.1 Numerical model

In this section, the three-dimensional (3D) numerical model of the new composite segment is set up via the ABAQUS program for numerical analysis. A total of four kinds of segment models were established, namely PT0, FH1, FH2 and FH3. The complete model of specimen PT0 consists of a concrete segment and a steel cage, and the complete models of specimens FH1, FH2 and FH3 consist of a concrete segment, a steel cage, a steel pipe and a concrete core.

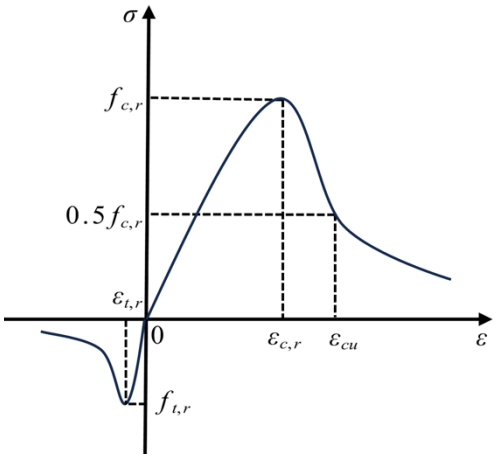

Fig. 2. Stress-strain curve of concrete materials

Hand holes and bolt holes are not included in the segment model, which simplifies the modeling process, ensures the regular geometry of the segment and an appropriate mesh shape, improves the computational efficiency of the model, and reduces convergence difficulties. In the segment model, both the concrete and steel pipes are modeled using 8-node linear brick elements with reduced integration (C3D8R), while the steel bars within the steel cage are represented by 2-node linear 3D truss elements (T3D2). The model of specimen FH1 after meshing is shown in Fig. 3.

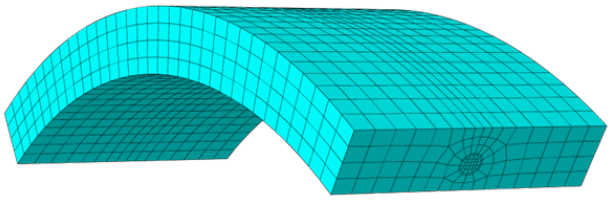

Fig. 3. Model of segment

Four different segments are modeled, all with identical dimensions. The outer radius and inner radii are 1500 mm and 1350 mm, respectively, while the width is 600 mm and the center angle is 67.5°. The steel used in these segments is of grade Q235B. The concrete for the four segments and the ASCFSP components is uniform, with a strength grade of C50.

The primary distinction among the four segments lies in the number of ASCFSP components incorporated within the inner segment. The ordinary segment, devoid of ASCFSP components, is designated as PT0. The three novel composite segments, containing one, two, and three ASCFSP components, are named FH1, FH2, and FH3, respectively. The installation positions of the steel bars and ASCFSP components within the segment cross-sections are illustrated in Fig. 4, where the numbers (1), (2), and (3) indicate the ASCFSP component installation positions for

the FH1, FH2, and FH3 specimens, respectively. Additionally, the installation positions of the circumferential steel bars and steel pipes within the segment are depicted in Fig. 5.

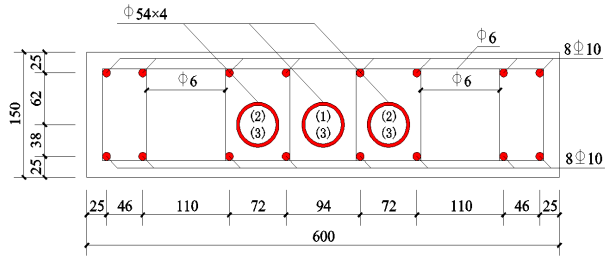

Fig. 4. Installed positions of the segment cross sections of the steel bars and ASCFSP components

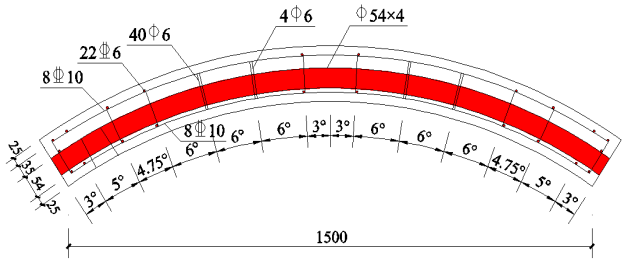

Fig. 5. Installed positions of the segments circumferential steel bars and steel pipes

To validate the numerical model, four scaled-down segments are tested: one ordinary segment and three new composite segments. The tests are conducted using a large self-reaction test frame with a measuring range of up to 1000 kN. A schematic diagram of the segment bending test is depicted in Fig. 6.

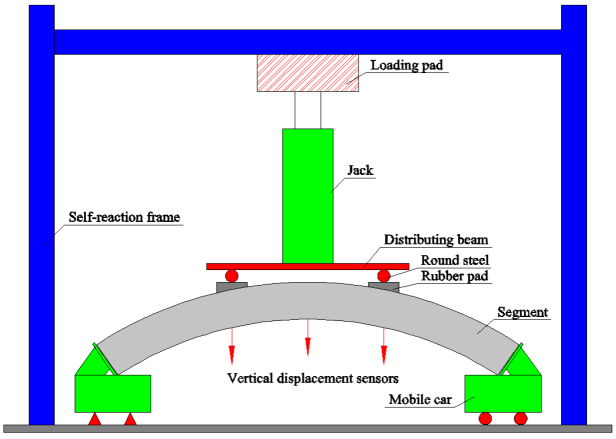

(a) Schematic drawing

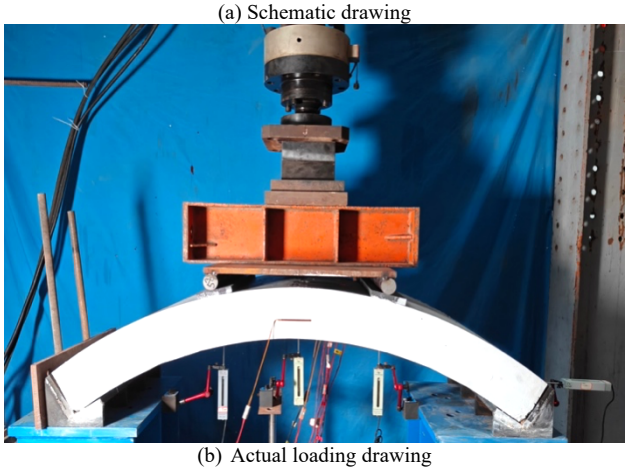

(b) Actual loading drawing

Fig. 6. Sketch of the segment bending performance test device

The loading mode employed is four-point loading, comprising two support points and two loading points. One end of the support is a fixed hinge, while the other end is a moving hinge, effectively simulating a simply supported beam configuration for the segment. The segment load is distributed into two points via a distribution beam mounted beneath the jack. Two round steel bars, with lengths matching the segment's width, are welded onto the distribution beam to ensure full-width coverage. To prevent local concrete crushing, two 20 mm-thick rubber pads are installed at the interface between the round steel bars and the segments. Vertical displacement sensors are positioned at the mid-span and loading points of the segment's inner arc to monitor vertical deformations.

The loading procedure for the segment is as follows: An initial preloading step involves applying a vertical load of 10 kN and holding it for 1 min. This load is then unloaded to 0 kN, and the process is repeated twice to eliminate any voids in the concrete and ensure complete contact between the segment and the support. Subsequently, formal loading commences. Initially, the load is increased to 80% of the design load in 20% increments of the design load. Next, the load is raised to 90% of the design load in 10% increments. Finally, the load is increased to the full design load in 5% increments, with each load level held for 5 min. Once the design load is reached, it is maintained for 30 minutes before continuing to load in 5% increments of the design load until the segment fails. Throughout the loading process, displacements are recorded, and the development and maximum width of cracks in the segment are observed and documented.

4. Results analysis and discussions

4.1 Model validation

The numerical results and experimental tests are compared in Fig. 7. As depicted in Fig. 7, the variation trends of the load-deflection responses between the four specimens and the simulations are essentially identical. This indicates that the models can be further utilized to simulate the mechanical behaviors of the segment. In the subsequent sections, an extended analysis is conducted based on the aforementioned numerical models.

4.2 Number of ASCFSP components

To gain a deeper understanding of the new composite segment proposed in this paper, a parametric study was conducted. In this section, the results of this study are introduced. The key parameters that affect the performance of the new composite segment are the number of ASCFSP components, pipe thickness, pipe diameter, and pipe position. The default material and geometric parameters used in the numerical models remain unchanged from those described in the Methodology section, unless specifically noted otherwise.

The segment models of the four specimens, PT0, FH1, FH2, and FH3, previously established, contain 0, 1, 2, and 3 ASCFSP components, respectively. The load-deflection curves obtained from the numerical calculations are presented in Fig. 8. These results clearly demonstrate that incorporating the ASCFSP component into the segment effectively enhances its load-bearing capacity, which aligns well with the aforementioned experimental findings.

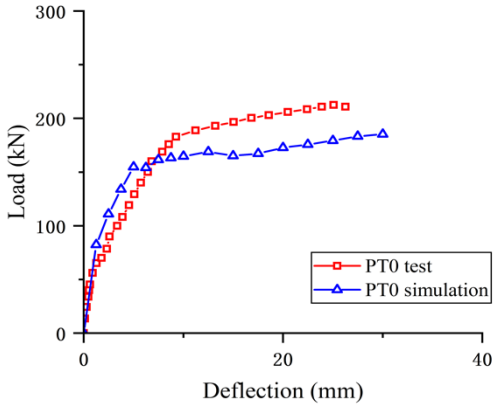

(a) Specimen PT0

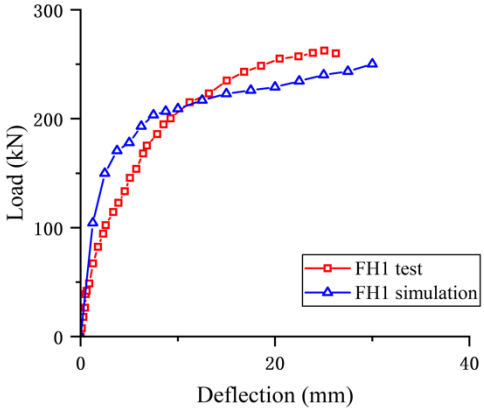

(b) Specimen FH1

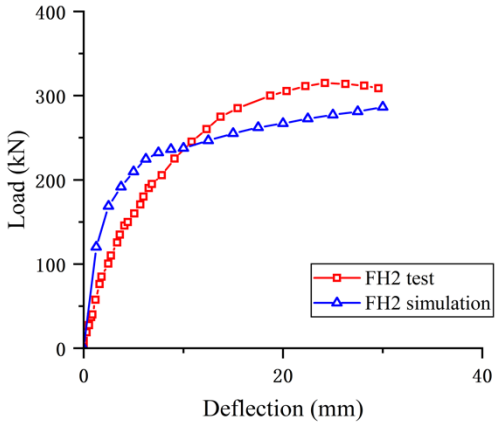

(c) Specimen FH2

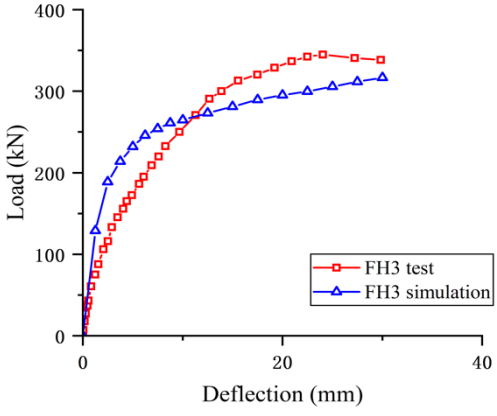

(d) Specimen FH3

Fig. 7. Comparison of the load-deflection curves between the tests and simulation results

To further investigate the influence of the ASCFSP component on the segment's load capacity, the numerical calculations revealed that the load capacities of the four specimen types (PT0, FH1, FH2, and FH3) were 185 kN, 250 kN, 287 kN, and 317 kN, respectively. Notably, incorporating 3 ASCFSP components into the segment resulted in a substantial 71.4% increase in load capacity. Further analysis showed that in the FH1, FH2, and FH3 models, the addition of each ASCFSP component led to load capacity increments of 35.1%, 27.6%, and 23.8%, respectively. This trend indicates that as the number of ASCFSP components in the segment increases, the individual contribution of each component to the overall load capacity gradually diminishes. However, it is clear that the addition of an ASCFSP component significantly enhances the segment's load capacity. Therefore, to optimize the utilization of the ASCFSP components in engineering applications, it is crucial to select the appropriate number of components based on the specific requirements and conditions.

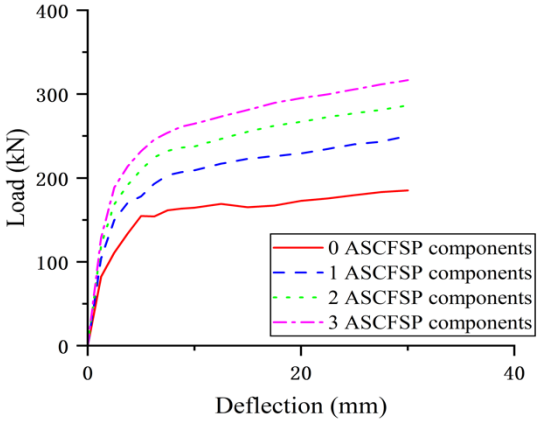

Fig. 8. Load-deflection responses of the segments with various numbers of ASCFSP components

4.3 Pipe thickness

To analyze the impact of pipe thickness on the segment's load capacity, the FH1 specimen model was selected for numerical analysis, with variations in pipe thickness (while keeping all other parameters constant). The pipe thickness was varied from 4 mm to 10 mm. The resulting load-deflection curves from the numerical calculations are presented in Fig. 9. The findings indicate that for every 2 mm increase in steel pipe thickness, the segment's load capacity increases by approximately 4%. This suggests that, although increasing pipe thickness does enhance the segment's load capacity, it is not a particularly efficient method for significantly improving its load-bearing capability.

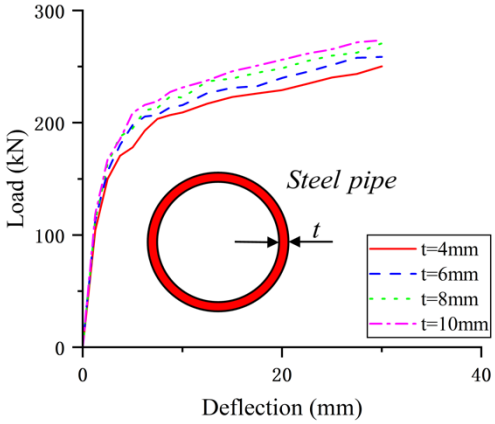

Fig. 9. Load-deflection responses of the segments with different steel pipe thicknesses

4.4 Outer diameter of the steel pipe

To examine the effects of pipe diameter on the segment's load capacity, the FH1 specimen model was selected for numerical analysis. The pipe diameter was varied, while keeping all other parameters constant, ranging from 54 mm to 66 mm. The resulting load-deflection curves, as presented in Fig. 10, reveal that the segment's load capacity increases by approximately 4% for every 4 mm increase in steel pipe diameter. Interestingly, this percentage increase is similar to that observed when increasing the pipe thickness. However, this suggests that increasing the pipe diameter, just like increasing the pipe thickness, is not a highly effective method for significantly improving the segment's load-bearing capacity.

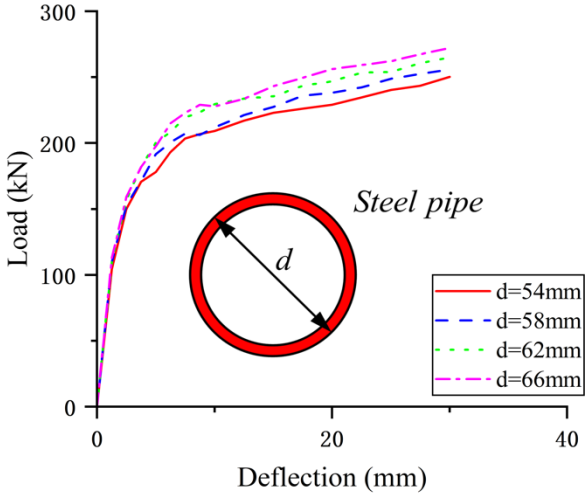

Fig. 10. Load-deflection curves of the segments with various steel pipe diameters

4.5 Position of the steel pipe

To investigate the influence of pipe position on the segment's load capacity, the FH1 specimen model was chosen for numerical analysis. The distance between the centroid of the pipe and the inner arc surface of the segment was varied, while keeping all other parameters constant, at distances of 63 mm, 78 mm, and 93 mm. The subsequent load-deflection responses, depicted in Fig. 11, indicate that altering the steel pipe's position has minimal impact on the segment's load capacity. This suggests that changing the pipe position does not serve as an effective means to enhance the mechanical performance of the segment.

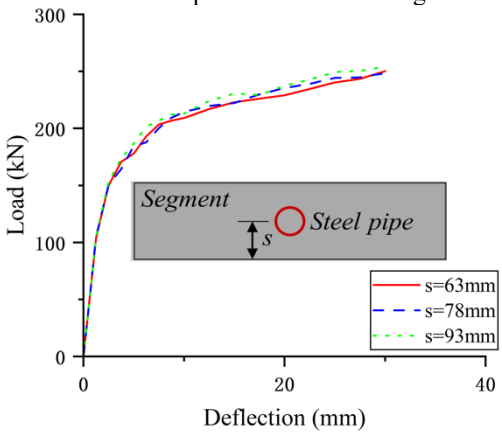

Fig. 11. Load-deflection responses of the segments with various positions in the pipe

5. Conclusions

In tunnel shield construction under complex geological conditions, a novel composite segment was introduced, and its mechanical properties were comprehensively investigated through modeling and laboratory testing. The main conclusions are obtained as following:

(1) Significantly Enhanced Load Capacity: Embedding the ASCFSP (Advanced Steel Fiber Reinforced Concrete or similar material) component into a conventional segment significantly boosts its load-bearing capacity. Specifically, the ultimate load capacities of the FH1, FH2, and FH3 segments were found to be 23.8%, 50%, and 64.3% higher, respectively, compared to the traditional PT0 segment. This finding indicates that the incorporation of ASCFSP components is an effective strategy for enhancing the load-bearing capacity of tunnel segments.

(2) Limited Impact on Cracking Load and Elevated Yield & Ultimate Loads: While the ASCFSP component does not significantly increase the cracking load of the segment, it does elevate the yield and ultimate loads to a certain extent. This suggests that after the segment begins to crack, the ASCFSP component more effectively distributes and bears the load, thereby delaying the overall failure of the structure.

(3) Relationship between Component Quantity and Load Capacity: For the novel composite segment, incorporating more ASCFSP components effectively boosts its load-bearing capacity. However, as the number of ASCFSP components increases, the contribution of each individual component to the load capacity gradually diminishes. Furthermore, the study revealed that pipe thickness and diameter have negligible effects on the segment's load capacity, and altering the steel pipe position does not significantly improve its load-bearing capacity. This underscores the importance of comprehensively considering component quantity and layout when designing and optimizing composite segments.

It is noteworthy that this study primarily focuses on the mechanical properties of the composite segment. However, in shield tunnels, the deformation of the segmental structure is influenced not only by the segments themselves but also by the joints connecting them. Therefore, future research should propose a new type of joint to further control the deformation of the tunnel lining. This new joint should possess excellent mechanical properties and durability to ensure the long-term stability and safety of the tunnel structure under complex geological conditions.

Acknowledgements

The work was fully supported by Fujian Province Guiding Project (2021Y0026).

References

[1] M. Maeda and K. Kushiyama, "Use of compact shield tunneling method in urban underground constructio," *Tunn. Undergr. Sp. Tech.*, vol. 20, no. 2, pp. 159-166, Mar. 2005. doi:10.1016/j.tust.2003.11.008.

[2] M. Z. Naghadehi, M. Thewes, and A. A. Lavasan, "Face stability analysis of mechanized shield tunneling: An objective systems approach to the problem," *Eng. Geol.*, vol. 262, Nov. 2019, Art. no. 105307. doi:10.1016/j.enggeo.2019.105307.

[3] T. Q. Wang, P. Geng, P. S. Li, Q. Wang, and L. J. Wang, "Deformation and failure of overburden soil subjected to normal fault dislocation and its impact on tunnel," *Eng. Fail. Anal*., vol. 142, Dec. 2022, Art. no. 106747. doi:10.1016/j.engfailanal.2022.106747.

[4] X. G. Wu, S. R. Wang, J. H. Yang, J. Q. Zhao, and X. Chang. "Damage characteristics and constitutive model of lightweight shale ceramsite concrete under static-dynamic loading," *Eng. Fract. Mech.*, vol. 259, Jan. 2022, Art. no. 108137. doi:10.1016/j.engfracmech.2021.108137.

[5] S. M. Hussaine and L. L. Mu, "Intelligent prediction of maximum ground settlement induced by EPB shield tunneling using automated machine learning techniques," *Mathmatics*, vol. 10, no. 24, Dec. 2022, Art. no. 4637. doi:10.3390/math10244637.

[6] K. Kinoshita and T. Ushida, "Numerical analysis method for corrosion of segment joints in shield tunnels caused by chloride tttack," *Q. Rep. RTRI*, vol. 64, pp. 242-247, Nov. 2023. doi: 10.2219/rtriqr.64.4_242.

[7] S. R. Wang, X. G. Wu, J. H. Yang, J. Q. Zhao, and F. L. Kong. "Mechanical behavior of lightweight concrete structures subjected to 3D coupled static-dynamic loads," *Acta Mech.*, vol. 231, no. 11, pp. 4497-4511, Aug. 2020. doi: 10.1007/s00707-020-02739-y.

[8] C. M. Monsberger, P. Bauer, F. Buchmayer, and W. Lienhart, "Large-scale distributed fiber optic sensing network for short and long-term integrity monitoring of tunnel linings," *J. Civ. Struct. Health*, vol. 12, no. 6, pp. 1317-1327, Dec. 2022. doi:10.1007/s13349-022-00560-w.

[9] B. Lyon, G. Candia, C. Gutiérrez, and J. Macedo, "Performance-based analysis of Transit tunnels in the Chilean subduction zone," *Soil Dyn. Earthq. Eng.*, vol. 152, Jan. 2022, Art. no. 107047. doi: 10.1016/j.soildyn.2021.107047.

[10] K. Nishikawa, "Development of a prestressed and precast concrete segmental lining," *Tunn. Undergr. Sp. Tech.*, vol. 18, no. 2-3, pp. 243-251, Apr. 2003. doi: 10.1016/S0886-7798(03)00033-6

[11] P. Vion and J. Joing, "Fabrication and erection of U-trough section bridges," *Struct. Eng. In.*, vol. 21, no. 4, pp. 426-432, Nov. 2011. doi: 10.2749/101686611X13131377725686.

[12] A. H. Varma, S. R. Malushte, K. C. Sener, and Z. C. Lai, "Steel-plate composite (SC) walls for safety related nuclear facilities: Design for in-plane forces and out-of-plane moments," *Nucl. Eng. Des.*, vol 269, pp. 240-249, Apr. 2014. doi: 10.1016/j.nucengdes.2013.09.019.

[13] Q. Zhao, F. Xiao, Y. Nie, Y.F. Yang, and X.M. Fang, "Behavior and design of steel-UHPC composite beams subjected to negative moment", *Structures*, vol. 57, Nov. 2023, Art. no. 105183. doi: 10.1016/J.ISTRUC.2023.105183.

[14] K. Yang, Q. X. Yan, and C. Zhang, "Three-dimensional mesoscale numerical study on the mechanical behaviors of SFRC tunnel lining segments," *Tunn. Undergr. Sp. Tech.*, vol. 113, Jul. 2021, Art. no. 103982. doi: 10.1016/J.TUST.2021.103982.

[15] A. M. Zeyad, I. S. Agwa, M. H. Abd-Elrahman, and S. A. Mostafa, "Engineering characteristics of ultra-high performance concrete containing basil plant ash" *Case Stud. Constr. Mat.*, vol. 21, Dec. 2024, Art. no. e03422. doi:10.1016/j.cscm.2024.e03422.

[16] X. G. Zhang, S. R. Wang, X. Gao, and Y. S. He, "Seismic behavior analysis of recycled aggregate concrete-filled steel tube column," *J. Eng. Sci. Technol. Re.*, vol. 12, no. 4, pp. 129-135, Aug. 2019. doi: 10.25103/jestr.124.16.

[17] A. Patchen, S. Young, and D. Penumadu, "An investigation of mechanical properties of recycled carbon fiber reinforced ultra-high-performance concrete" *Materials*, vol. 16, no. 1, Jan. 2023, Art. no. 314. doi:10.3390/ma16010314.

[18] Y. Zhang, S. Cai, Y. Zhu, L. Fan, and X. Shao, "Flexural responses of steel-UHPC composite beams under hogging moment," *Eng. Struct.*, vol. 206, Mar. 2020, Art. no. 110134. doi: 10.1016/j.engstruct.2019.110134.

[19] A. H. Alani, M. A. M. Johari, A. T. Noaman, N. M. Bunnori, and T. A. Majid, "The role of silica fume in enhancing the strength and transport properties of PET fiber-ultra high-performance concrete," *Adv. Civ. Eng. Mater.*, vol. 13, no. 1, pp. 95-115, May 2024. doi:10.1520/ACEM20230036.

[20] B. Swathi and R. Vidjeapriya, "Influence of precursor materials and molar ratios on normal, high, and ultra-high performance geopolymer concrete-A state of art review," *Constr. Build. Mater.*, vol. 392, Aug. 2023, Art. no. 132006. doi:10.1016/j.conbuildmat.2023.132006.

[21] D. M. Zhang, D. M. Zhang, K. Soga, H. W. Huang, and F. Wang, "Rehabilitation of overdeformed metro tunnel in shanghai by multiple repair measures," *J. Geotech. Geoenviron. Eng.*, vol. 145, no. 11, Nov. 2019, Art. no. 04019101. doi: 10.1061/(ASCE)GT.1943-5606.0002169.

[22] X. H. Zhang, Z. R. Lin, K. P. Zhang, H. G. Di, C. He, and S. H. Zhou, "Full-scale experimental test for load-bearing behavior of the carbon fiber shell reinforced stagger-jointed shield tunnel," *Compos. Struct.*, vol. 311, May 2023, Art. no. 116773. doi: 10.1016/j.compstruct.2023.116773.

[23] T. T. Lai, M. K. Kim, V. D. Truong, T. U. Kim, and D. J. Kim, "Electromechanical response of smart ultra-high-performance concrete beams under flexure: Effects of filler type and electrode spacing," *Cement Concrete Comp.*, vol. 152, Sept. 2024, Art. no. 105629. doi:10.1016/j.cemconcomp.2024.105629.

[24] J. Pachman, D. J. Chapman, M. Foglar, M. Künzel, and W. G. Proud, "Shock response of concrete, fibre concrete and ultrahigh performance concrete," *Int. J. Impact Eng.*, vol. 183, Jan. 2024, Art. no. 104787. doi:10.1016/j.ijimpeng.2023.104787.

[25] X. D. Shao, H. Q. Zeng, and J. H. Cao, "Flexural behavior of fully prefabricated large cantilevered high strength steel-UHPC composite bent caps," *J. Constr. Steel Res.*, vol. 204, May 2023, Art. no. 107856. doi: 10.1016/J.JCSR.2023.107856.

[26] G. Tiberti, F. Minelli, and G. Plizzari, "Reinforcement optimization of fiber reinforced concrete linings for conventional tunnels." *Compos. Part B-Eng.*, vol. 58, pp. 199-207, Mar. 2014, doi: 10.1016/j.compositesb.2013.10.012.

[27] X. Liu, Z. J. Jiang, and H. Mang, "Experimental investigation of the bearing capacity of deformed segmental tunnel linings strengthened by a special composite structure," *Struct. Infrastruct. Eng.*, vol. 19, no. 2, pp. 147-163, Nov. 2021. doi: 10.1080/15732479.2021.1924796.

[28] W. Naguib and A. Mirmiran, "Creep modeling for concrete-filled steel tubes," *J. Constr. Steel Res.*, vol. 59, no. 11, pp. 1327-1344, Nov. 2003. doi:10.1016/S0143-974X(03)00085-3.

[29] E. Inai, A. Mukai, M. Kai, H. Tokinoya,T. Fukumoto, and K. Mori, "Behavior of concrete-filled steel tube beam columns," *J. Struct. Eng.-ASCE*, vol. 130, no. 2, pp. 189-202, Feb. 2004. doi:10.1061/(ASCE)0733-9445(2004)130:2(189).

[30] C. W. Roeder, D. E. Lehman, and M. Stephens, "Concrete-filled steel tubes for accelerated bridge construction," *Trandport. Res. Rec*., no. 2046, pp. 49-58, Sept. 2014. doi:10.3141/2406-06.